ELSEVIER

Journal of the Mechanics and Physics of Solids
52 (2004) 999–1022

JOURNAL OF THE
MECHANICS AND
PHYSICS OF SOLIDS

www.elsevier.com/locate/jmps

Tensile and mixed-mode strength of a thin film-substrate interface under laser induced pulse loading

Junlan Wang*, Nancy R. Sottos, Richard L. Weaver

Department of Theoretical and Applied Mechanics, University of Illinois, Urbana-Champaign 216 Talbot, 104 S. Wright, Urbana, IL 61801, USA

Received 21 March 2003; received in revised form 22 September 2003; accepted 22 September 2003

Abstract

Laser induced stress waves are used to characterize intrinsic interfacial strength of thin films under both tensile and mixed-mode conditions. A short-duration compressive pulse induced by pulsed-laser ablation of a sacrificial layer on one side of a substrate is allowed to impinge upon a thin test film on the opposite surface. Laser-interferometric measurements of test film displacement enable calculation of the stresses generated at the interface. The tensile stress at the onset of failure is taken to be the intrinsic tensile strength of the interface. Fused-silica substrates, with their negative nonlinear elasticity, cause the compressive stress wave generated by the pulse laser to evolve a decompression shock, critical for generation of the fast fall times needed for significant loading of surface film interfaces. By allowing the stress pulse to mode convert as it reflects from an oblique surface, a high amplitude shear wave with rapid fall time is generated and used to realize mixed-mode loading of thin film interfaces. We report intrinsic strengths of an aluminum/fused silica interface under both tensile and mixed-mode conditions. The failure mechanism under mixed-mode loading differs significantly from that observed under pure tensile loading, resulting in a higher interfacial strength for the mixed-mode case. Inferred strengths are found to be independent, as they should be, of experimental parameters.

Keywords: Thin film; Interfacial adhesion; Mixed-mode loading; Laser pulse; Stress waves

* Corresponding author. Department of Mechanical Engineering, Bourns College of Engineering, University of California, Riverside, CA 92521, USA. Tel.: +1909-787-6429; fax: +1909-787-2899.
E-mail address: wang@engr.ucr.edu (J. Wang).

0022-5096/$ - see front matter © 2003 Elsevier Ltd. All rights reserved.
doi:10.1016/j.jmps.2003.09.029

1. Introduction

Thin films are crucial components in a wide range of multilayer microelectronic and optical devices. The size scales and dissimilar nature of the constituents present great challenges for thermomechanical integrity and reliability (Evans and Hutchinson, 1995). Of particular importance is the design and implementation of test procedures that measure thin-film interface properties.

Interfacial adhesion influences the mechanical behavior and reliability of a thin film on a substrate. In many practical applications of thin films, the level of adhesion required for the thin film structure depends on the severity of the operating environment. For an ideal planar interface, the intrinsic adhesion corresponds to the summation of all atomic and molecular bonding forces acting between the adjoining material surfaces. In practice, however, the interfacial region can depend on many parameters, such as substrate surface morphology, chemical inter-diffusion, contamination, and defects (Mittal, 1978, 1987; Mattox, 1978; Alexopoulos and O'Sullivan, 1990). Testing interfacial adhesion typically involves applying external loads by some means to the surface of the film and generally results in a complex stress field at the interface because of the load-application mechanism, the dissimilar materials involved, and often large induced deformations.

Significant effort has been devoted to the development of test procedures for the measurement of thin-film adhesion, of which the most common are the scratch, peel, pull, blister, and indentation tests. The first quantitative use of the scratch test was reported by Heavens (1950) and Weaver (1975). Later this method was widely adopted for characterizing the adhesion and mechanical durability of thin hard films, which typically have a high adhesion strength (Laugier, 1981; Hull et al., 1987). In the scratch test, a conical diamond indenter is dragged across a film sample until a load drop occurs, indicating delamination. The scratch test is simple, but extracting a quantitative adhesion value has proven to be difficult (Hull et al., 1987). Both the testing parameters (loading rates, stylus radius) and the sample parameters (film thickness and substrate hardness) influence the test results. Thus, the scratch test usually provides only a comparative measure of interfacial strength.

In the peel test, first used by Strong (1935), an adhesive layer is bonded to the film surface and lifted off, potentially removing the film. In an alternative version of this test (super layer delamination technique), another thicker layer is deposited on the thin film and the residual stress in that layer causes the film to delaminate from the substrate (Baglin and Clark, 1985). Peel strength depends on many parameters, including film thickness and substrate compliance, and can involve substantial elastic–plastic deformation of the film (Kim and Kim, 1988). The peel test is suitable only for films in which the adhesion to the substrate is weaker than to the adhesive layer. For cases where the adhesion is considerably higher, the pull test (Hull et al., 1987; Jacobsson and Kruse, 1973) is often used. In a pull test, a stud is attached to the film using a strong adhesive. The perpendicular force required to remove the stud is measured and then divided by the area of removed film to calculate the adhesive strength. A major limitation of the pull test is that the maximum measurable strength cannot exceed the maximum bonding strength of available adhesives. In both the peel

and pull tests the potential exists that the adhesive used to attach the stud will penetrate the film and affect the film and interface.

Another technique used for thin-film adhesion measurement is the blister test, in which a film layer is deposited on a rigid flat substrate with a center perforation. A pressurizing fluid is injected through the perforation creating a blister and causing a progressive debonding of the film/substrate interface at a critical pressure (Gent and Lewandowski, 1987; Chu et al., 1992). Blister tests usually require time consuming sample preparation procedures. Indentation-induced delamination has also been proposed for measuring film adhesion (Kriese et al., 1999a,b). As in the scratch test, a diamond indenter is used to initiate and propagate a delamination, which is then examined optically and related to the measured load and displacement. Indentation tests are difficult when applied to ductile or strongly adhering films because of the problem of initiating a delamination (Turner and Evans, 1996). During all these tests — scratch, peel, pull, blister and indentation — the interface is subjected to very high stress levels and consequent inhomogeneous deformations. Large amounts of plastic deformation can result (especially in the peel test) and dominate the behavior during the test (Thouless, 1994). Although these tests are simple to perform and useful for basic adhesion characterization, the stress fields are difficult to analyze and the resulting adhesion measurements tend to be qualitative and provide a more comparative assessment.

Different from these methods, laser-spallation methods load the interface in a remote, non-contacting manner using laser-generated stress waves. This technique, introduced by Yang (1974) and later extended by Vossen (1978), involves impinging a high-energy laser pulse (with a duration of nanoseconds) from a Q-switched laser onto a thin absorbing layer located between a transparent confining plate and the back surface of the substrate. Upon absorbing the laser energy, the sudden expansion of the confined layer generates a compressive stress wave directed towards the test film. The reflection of the compressive wave packet from the surface of the test film generates a tensile pulse, which leads to spallation of the test film. Yang (1974) used an x-cut quartz crystal to measure the stress at the front surface of the substrate.

Gupta and co-workers (Gupta et al., 1990, 1992) further developed Vossen and Yang's technique to measure thin-film interfacial strength. As in Yang's work (1974), the stress impinging the interface was measured using a microelectronic device with an x-cut piezoelectric crystal. In the later work of Gupta et al. (Gupta and Yuan, 1993; Gupta et al., 1994; Yuan and Gupta, 1993; Yuan et al., 1993), a laser-Doppler interferometer was introduced to measure the free-surface displacement and velocity, which were then related to interface stress. This technique was used to measure the tensile strength of a wide variety of metal/ceramic (Gupta and Yuan, 1993, Gupta et al., 2000), ceramic/ceramic (Gupta et al., 1994), thermal-barrier coatings (Gupta and Yu, 1997), ice/metal (Archer and Gupta, 1998) and fiber/matrix (Yu and Gupta, 1998) interfaces. More recently, Boustie et al. (1999) used the laser-spallation technique to test adhesion of some metal/metal film interfaces with film thicknesses on the order of tens of micrometers. In their tests, upper and lower laser-intensity thresholds for spallation generation were determined experimentally and a traction range for debonding at the interface was determined numerically.

In all the laser spallation experiments reported in the literature, only normal pressure pulses were applied to the films. Consequently, the interfaces were subjected only to tensile (mode I) loading. In most commercial applications, however, thin-film interfaces fail under mixed-mode conditions (Evans and Hutchinson, 1995). Design of experiments to measure the interface debonding over a range of mode mixity relevant to practical problems is a significant challenge. Several test methods for characterizing mixed-mode interfacial fracture of a bilayer have been proposed in literature, such as mixed-mode double cantilever beam (Thouless, 1990), double cantilever drilled compression (Evans and Hutchinson, 1995), mixed-mode flexure (Charalambides et al., 1989; Cao and Evans, 1989; Sbaizero et al., 1990; Evans et al., 1991), and Brazil-nut specimen (Wang and Suo, 1990). Most of these test methods involve sandwich configurations in which a film is deposited onto two substrates and subsequently bonded together before adhesion measurement. The bonding process requires diffusion either at relatively high homologous temperatures or under applied pressure, and often leads to changes at the interface and in the microstructure of the film. Thus, the bonding process plays a role in the nature and the magnitude of the energy-dissipative mechanisms. Measurement using these sandwiches is even more problematic for thin-film interfaces produced at relatively low temperatures (e.g., by sputtering or evaporation) due to difficulty loading the film in a controlled manner at the relevant phase angle. Since the film is sandwiched between two substrate materials, it is also difficult to examine the damage pattern resulting from interface failure.

Recently, Wang et al. (2002, 2003a) carried out a systematic parametric study on the tensile laser spallation technique and extended it to the study of the mixed-mode interfacial failure of thin films using laser-generated stress waves. With the new technique, the mixed-mode interfacial adhesion of a surface film deposited on a substrate is measured in the as-processed condition, which differs significantly from the sandwich specimens adopted in the literature.

In this paper, the adhesion strength of an Al film/fused silica substrate interface is measured using both tensile laser spallation and the newly developed mixed-mode loading experiments and the values are compared with each other. The Al/fused silica interface is studied as a model system because fused silica has the desirable characteristics in terms of shock formation. With a simple insertion of any other substrate material between the test film and fused silica substrate, the adhesion strength between any pairs of materials can be studied.

2. Tensile failure of Al/fused silica interface

Although the tensile spallation technique has received extensive attention from Gupta and co-workers (Gupta and Yuan, 1993; Yuan and Gupta 1993; Yuan et al., 1993; Gupta et al., 1994), the past work has largely focused on evaluating film adhesion, with questions relating to optimal experiment design given less analysis. With a view towards the optimal design for the mixed-mode loading experiment, a systematic investigation of the effect of various parameters governing the wave generation mechanisms was carried out in the tensile case. The tensile strength of Al/fused silica interface was measured

using different thicknesses of films and substrates for the purpose of comparison with later mixed-mode failure strength.

2.1. Tensile spallation experiment

Fig. 1 shows the basics of the stress wave generation in the tensile loading experiment. The thin film sample consists of (from left to right): a confining layer (CL), a thin energy absorbing layer (AL), a substrate (S) and a test film (F). An infra-red, Nd:YAG laser pulse ($\lambda = 1064$ nm) with a variable energy content between 1 and 110 mJ, and a rise time of order of 5 ns is incident on a metallic absorbing layer sandwiched between the confining layer and substrate. The energy-absorbing layer is chosen to be much thicker (typically 0.5 μm) than the critical penetration depth (on the order of tens of nanometers) of laser light at this wavelength. When the laser energy is deposited at the interface of the confining layer and the energy-absorbing layer, a longitudinal stress wave of rise time comparable to that of the laser pulse is emitted from the metallic layer. The wave that propagates towards the film/substrate interface is then reflected back from the film free surface into a tensile wave, which then loads the test interface in tension. The nominal diameter of the YAG laser beam used in the current project is 3.5 mm. In order to increase the laser fluence, the laser beam is focused onto a 1 mm diameter spot on the energy-absorbing layer. The laser energy is increased until a longitudinal wave is generated with an amplitude sufficient to fail the film/substrate interface.

Interferometric measurements of out-of-plane displacement are made at the surface of the test film. From displacement measurements at the free surface, the stress history in the substrate and at the interface can be inferred using standard wave mechanics (Miklowitz, 1978). For a small film thickness h (smaller than the wave speed times the rise time of the stress pulse), the stresses can be calculated (Wang et al., 2002) using the following equations:

$$\sigma_{\text{sub}} = -\frac{1}{2}(\rho c)_{\text{sub}} \frac{\partial u}{\partial t}, \tag{1}$$

$$\sigma_{\text{int}} = -(\rho h)_{\text{film}} \frac{\partial^2 u}{\partial t^2}, \tag{2}$$

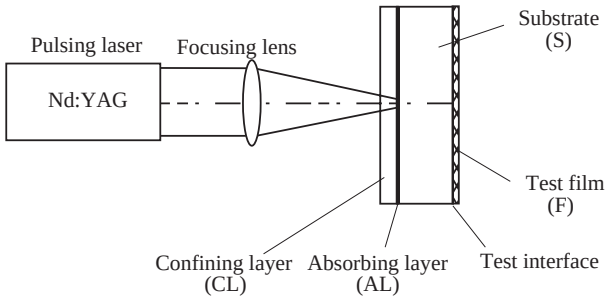

Fig. 1. Schematic of the tensile laser-spallation technique.

where σ_{sub} and σ_{int} are the stresses acting in the substrate and at the interface, respectively; u is the measured out-of-plane displacement of the test film, ρ is density and $c = 5.94 \times 10^3$ m/s is the longitudinal wave speed for our fused silica. For the case in which the film thickness h is large, an exact solution based on wave transmission and reflection coefficients is provided in Appendix A. For the film thickness investigated in present work, the approximate calculation (Eq. (2)) gives the same result as the exact solution.

The spallation behavior of Al thin films was investigated by Wang et al. (2002) as a function of substrate thickness, film thickness, laser energy and various parameters governing the source. Two different substrate materials, single crystal Si (1 0 0) and fused silica, were considered. The interface stress increased with laser power, film thickness, confining layer thickness, but decreased with substrate thickness due to geometric attenuation caused by the finite size of the YAG beam.

The most significant achievement of this tensile spallation parametric study, was the identification of a laser-induced weak shock formation in fused silica substrate. Due to the negative nonlinear elasticity of fused silica, a laser-induced Gaussian stress pulse evolved into a shock after travelling a certain distance in a fused silica substrate, which was highly beneficial for realizing significant loading at the thin-film interface. A rigorous theoretical analysis of the shock development mechanism in fused silica and the various parameters influencing shock detection in the laser spallation experiment was provided in Wang et al. (2003b).

To illustrate the experimental procedure, Fig. 2 shows typical interferometric data obtained from a 0.5 μm thick aluminum film vapor deposited on a 1500 μm fused silica substrate with waterglass confining layer thickness of 0.4 μm at the full YAG power (0.140 J/mm^2). The unprocessed fringe data is plotted in Fig. 2a. Within 40 ns, almost 10 fringes developed corresponding to a total displacement of 2.57 μm. In the first 22 ns, the fringe spacing becomes tighter and tighter, indicating acceleration in surface velocity. With a sudden turning (velocity direction change) at 22 ns, the fringe spacing becomes larger and larger indicating a deceleration in surface velocity. From Fig. 2a, the out-of-plane displacement of the test film surface is calculated (one fringe corresponds to a surface displacement of one half optical wavelength). The corresponding stress in the fused silica substrate is then calculated using Eq. (1) and shown in Fig. 2b. The steady increase in surface velocity corresponds to a linear ramp in the substrate stress. This ramp is due to the nonlinear elasticity of the fused silica substrate, softening at compressive strains up to 5% and stiffening at higher strains. This behavior is consistent with previous studies of shocks using flyer plate impact experiments (Barker and Hollenbach, 1970). The sudden change in surface velocity at 22 ns corresponds to a sharp shock at the turning point. A maximum compressive stress of 1.2 GPa is achieved in the substrate. For a 0.5 μm thick aluminum film, a small amount of film failure is observed at the full YAG power with a measured maximum interfacial stress of 420 MPa.

More significant damage is generated when thicker films are tested. Fig. 4 contains photographs of typical damage patterns observed for a 0.9 μm film deposited on 1500 μm thick fused silica substrate. The film fails in a blister-like fashion with many distinct “finger-like” regions. The number of fingers increases with increasing laser

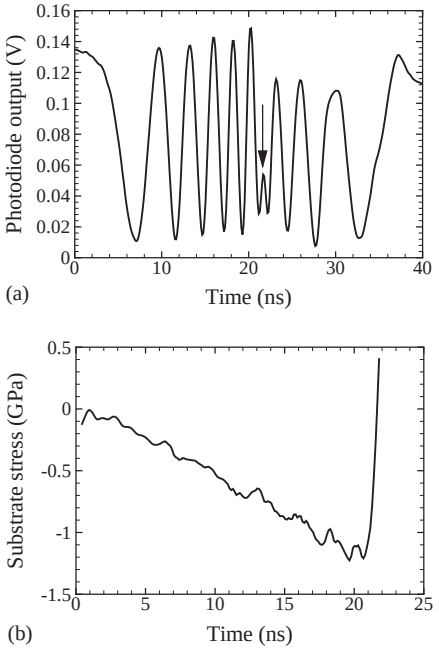

Fig. 2. Interferometric signal obtained for a 0.5 μm thick aluminum film deposited on a 1500 μm thick fused-silica substrate with 0.4 μm thick waterglass (laser fluence of 0.140 J/mm^2): (a) photodiode output; and (b) substrate stress. Arrow points to the position where fringes suddenly changed direction.

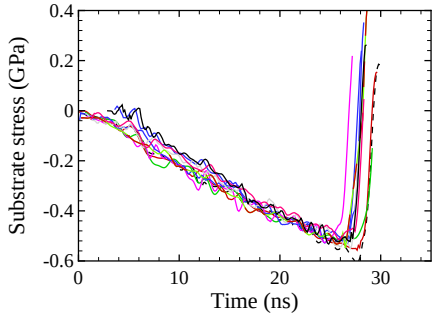

Fig. 3. Substrate stress profile for a 1.8 μm thick aluminum film deposited on a 3000 μm thick fused silica substrate.

fluence because at higher laser fluence, more energy is stored in the film, resulting in more blistering. The symmetry of the failure pattern reflects the uniformity of the loading. Variations in the film, interface or pulse generation may lead to unsymmetric failure.

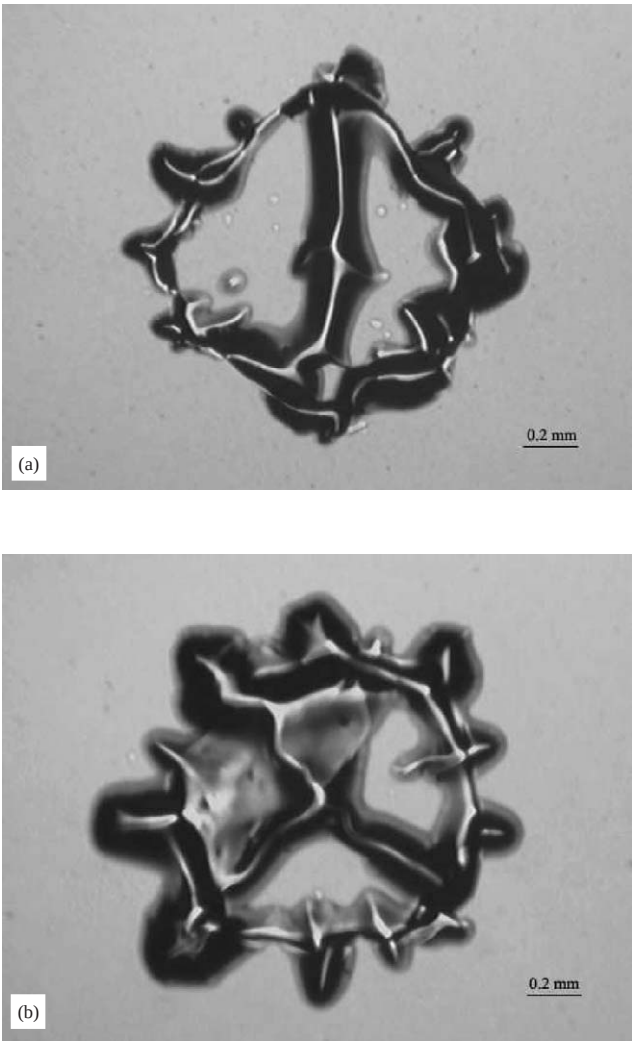

Fig. 4. Damage development for a 0.9 μm thick aluminum film deposited on 1500 μm thick fused silica substrate: (a) laser fluence at 0.084 J/mm^2 and (b) laser fluence at 0.140 J/mm^2.

2.2. Tensile strength of Al/fused silica interface

The interfacial strength of aluminum/fused silica was measured on both 1500 μm and 3000 μm fused silica substrates with different film thickness. The YAG power was gradually stepped up until a small amount of damage was initiated at the film interface. For the 3000 μm fused-silica substrate, an aluminum test film of 1.8 μm thickness was used to characterize the interfacial strength. Film failure initiated at full laser power

Table 1
Tensile strength of a 1.8 μm thick aluminum film deposited on a 3000 μm thick fused silica substrate

Test No.	Laser fluence (J/mm^2)	Substrate stress[a] (GPa)	Interface stress[a] (MPa)
1		−0.61	435
2		−0.55	460
3		−0.54	492
4		−0.57	462
5		−0.55	480
6	0.140	−0.59	478
7		−0.53	470
8		−0.58	532
9		−0.60	511
10		−0.54	505
11		−0.52	462
Range	0.140	−(0.53–0.61)	435–532
Average	0.140	-0.57 ± 0.03	481 ± 28

[a]Calculated using Eqs. (1) and (2) valid for small film thickness.

($0.140\ J/mm^2$). The maximum substrate and interface stress for tests performed at 11 different spots on the same sample are summarized in Table 1. To show the consistency of these experiments, substrate stress profiles for the 11 tests are plotted together in Fig. 3. The maximum substrate stress and interface stress were calculated using Eqs. (1) and (2). At film failure, the maximum substrate stress was 0.57 ± 0.03 GPa. The maximum interface stress was 481 ± 28 MPa.

In the case of the 1500 μm thick fused-silica substrate, two aluminum film thicknesses, 0.5 and 1.8 μm, were studied. For the 0.5 μm thick film, most failure initiated at full laser power ($0.140\ J/mm^2$). For the 1.8 μm thick film, failure initiated at a lower laser fluence of $0.084\ J/mm^2$. The maximum substrate stress and maximum interface stress calculated using Eqs. (1) and (2) for 5 tests performed at different spots are summarized in Tables 2 and 3, respectively. For the 0.5 μm thick film, the interface failed at an average maximum substrate stress of −1.1 GPa and interface stress of 497 MPa. For the 1.8 μm thick film, the interface failed at an average maximum substrate stress of −0.58 GPa and interface stress of 492 MPa. Tables 1–3 indicate that for different film thicknesses and different substrate thicknesses, the interface strength of aluminum/fused silica is approximately the same, 481 ± 28 MPa for 1.8 μm film on 3000 μm substrate, 497 ± 70 MPa for 0.5 μm film on 1500 μm substrate and 492 ± 55 MPa for 1.8 μm film on 1500 μm substrate. This is a very satisfactory result. Interface strength is independent of experimental parameters. Furthermore, and as expected, failure correlates with inferred interface stress, not substrate stress. For the same film thickness on different substrate thickness, the maximum substrate and interface stress are the same, but lower laser fluence is required for the thinner substrate, probably due to the reduced stress wave attenuation in the thinner substrates. For different film thicknesses

Table 2
Tensile strength of a 0.5 μm thick aluminum film deposited on a 1500 μm thick fused-silica substrate

Test No.	Laser fluence (J/mm^2)	Substrate stress (GPa)	Interface stress (MPa)
1		−1.1	583
2		−1.1	502
3	0.140	−1.2	420
4		−1.1	547
5		−1.1	435
Range	0.140	−(1.1–1.2)	420–583
Average	0.140	-1.1 ± 0.05	497 ± 70

Table 3
Tensile strength of a 1.8 μm thick aluminum film deposited on a 1500 μm thick fused-silica substrate

Test No.	Laser fluence (J/mm^2)	Substrate stress (GPa)	Interface stress (MPa)
1		−0.55	429
2		−0.62	474
3	0.084	−0.55	525
4		−0.61	568
5		−0.55	465
Range	0.084	−(0.55–0.62)	429–568
Average	0.084	-0.58 ± 0.04	492 ± 55

on the same substrate thickness, thicker films require less laser fluence, and consequently lower substrate stress to fail. This result is consistent with the predictions from Eqs. (1) and (2), higher stress is generated in thicker films.

3. Mixed-mode failure of Al/fused silica interface

3.1. Mixed-mode loading experiment

According to wave propagation and mode conversion theory, a mixed-mode loading experiment may be accomplished by modifying the sample geometry so that a high-strain-rate shear wave is generated by mode conversion at an oblique surface and then allowed to impinge upon the test film. A diagram describing the generation of high-amplitude, short-duration shear waves is shown in Fig. 5. Similar to the tensile spallation experiment, the sample consists of a transparent confining layer, a thin energy absorbing layer, a substrate and a test film. In order to generate a high amplitude shear wave, the planar substrate in the tensile spallation is replaced with a triangular

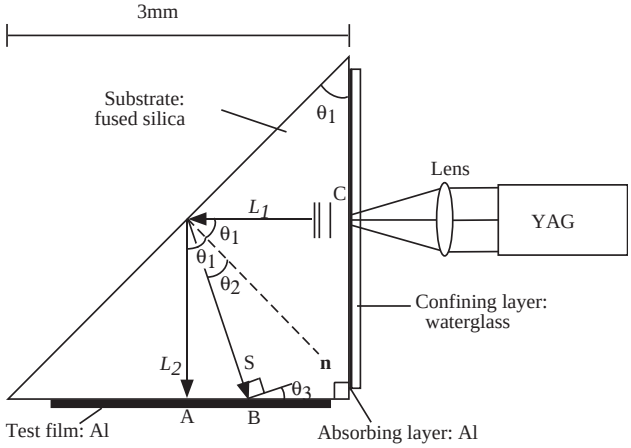

Fig. 5. Configuration for laser generated shear waves.

prism. The same infrared Nd:YAG pulse ($\lambda = 1064$ nm) as was used in the tensile case is incident on the absorbing layer at point C. Again, in order to increase the laser fluence, the laser beam is focused to a 1 mm diameter spot on the energy-absorbing layer.

When the laser pulse reaches the absorbing layer, a longitudinal compressive stress wave, L_1, of rise time comparable to that of the laser pulse is emitted from the absorbing layer. It propagates and evolves a shock and is reflected at the oblique surface. A major fraction of its energy—the exact amount depends on details of the angle θ_1 and the material elastic constants—is mode-converted into a shear wave, S. A smaller amount reflects as a longitudinal wave, L_2. The two reflected waves are then incident—propagation direction depends on the precise choice of θ_1—upon the test film surface at points B and A, respectively.

Fig. 5 shows the angles θ_1 and θ_2 between the normal to the oblique surface, n, and the propagation directions of the longitudinal and shear waves; θ_3 is the angle between the shear wave displacement (displacement is normal to the propagation direction of the shear wave) and the test film; $\theta_3 = \theta_1 - \theta_2$. The displacement amplitudes of the incident longitudinal, reflected longitudinal and shear waves are denoted with u_{L_1}, u_{L_2} and u_S. According to standard wave propagation theory (Graff, 1991) and the material properties of fused silica substrate, at an incident angle of $\theta_1 = 45°$, the mode conversion coefficient from incident longitudinal wave L_1 to shear wave S is nearly at a maximum, i.e., more than 99% of the energy of the incident longitudinal wave, L_1, is mode-converted into the shear wave, S (details of the mode conversion coefficients and the determination of angle $\theta - 1$ is provided in Appendix B). Using Snell's law, the angle of the reflected shear wave is calculated $\theta_2 = 26.5°$, so $\theta_3 = 18.5°$. In this configuration, the reflected longitudinal wave will be incident at point A normal to the test film surface and all of the amplitude of the longitudinal displacement will contribute to the measured out-of-plane motion at point A. The corresponding shear

wave arrives at the test film surface at point B, where only one part of the shear wave displacement contributes to the out-of-plane motion.

Based on the previous analytical analysis of wave attenuation with respect to substrate thickness (Wang et al., 2002), the lengths of the orthogonal sides of the triangular cross-section in Fig. 5 are chosen to be 3 mm. With the YAG beam incident at the center of the 3 mm wide absorbing layer surface, the distance between points A and B is found to be approximately 0.5 mm. However, for a 1 mm diameter YAG spot, the diameter of the wave front of the longitudinal wave is also 1 mm (centered at point A) and the diameter of the wave front of the shear wave is slightly larger, about 1.33 mm (centered at point B). Thus within region AB, the signals from the reflected longitudinal and shear waves are overlapped. Due to the arrival time difference, these two waves are readily distinguished (Wang et al., 2003a).

A Michelson interferometer is again used to detect the out-of-plane motion of the test film surface. By focusing the argon detection beam at a point between A and B (Fig. 5), a longitudinal wave, L_2, and a shear wave, S, will be detected. The displacements in the substrate u_{L_2} and u_s can be obtained directly from the out-of-plane interferometric measurements at any point between A and B. Note that in the experiment, the wave displacements u_s and u_{L_2} in the substrate are not measured directly; rather, the out-of-plane displacement of the film, $u_\perp$ (Eq. (B.7)) and $2u_{L_2}$ are actually measured. Once the displacements are obtained, the corresponding stresses in the substrate and at the interface are calculated according to

$$\sigma_{\text{sub}}^{L_2} = -(\rho c_L)_{\text{sub}} \frac{\partial u_{L_2}}{\partial t}, \tag{3}$$

$$\tau_{\text{sub}}^{S} = -(\rho c_S)_{\text{sub}} \frac{\partial u_S}{\partial t}, \tag{4}$$

$$\sigma_{\text{int}}^{L_2} = -2(\rho h)_{\text{film}} \frac{\partial^2 u_{L_2}}{\partial t^2}, \tag{5}$$

$$\tau_{\text{int}}^{S} = -(\rho h)_{\text{film}} \frac{\partial^2 u_{\parallel}}{\partial t^2} = -(\rho h)_{\text{film}} \frac{\partial^2 u_S \beta\gamma}{\partial t^2}, \tag{6}$$

$$\sigma_{\text{int}}^{S} = -(\rho h)_{\text{film}} \frac{\partial^2 u_{\perp}}{\partial t^2} = -(\rho h)_{\text{film}} \frac{\partial^2 u_S \beta}{\partial t^2}, \tag{7}$$

where $\sigma_{\text{sub}}^{L_2}$ and τ_{sub}^{S} are the normal and shear stress amplitudes of the waves in the substrate, $\sigma_{\text{int}}^{L_2}$ is the interface tensile stress induced by the longitudinal wave L_2 at point A (Fig. 5), τ_{int}^{S} is the interface shear stress induced by the shear wave S at point B, σ_{int}^{S} is the interface tensile stress induced by the shear wave S at point B (Fig. 5), ρ is density, c_L and c_S are the longitudinal and shear wave speed of fused silica substrate, respectively ($c_S = 3.75 \times 10^3$ m/s as provided by the manufacturer); h is the test

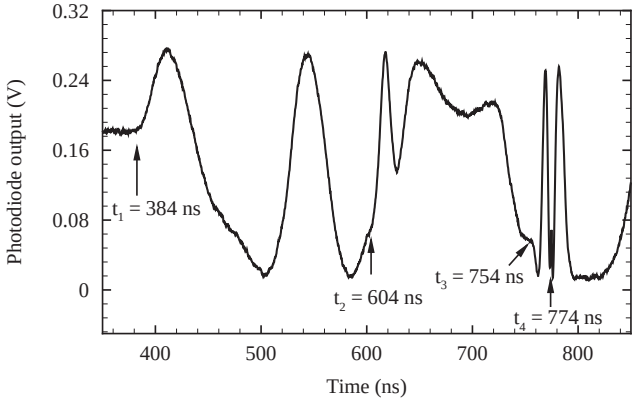

Fig. 6. Typical interferometric data obtained on a 1.0 μm thick Al film at point B.

film thickness, β and γ are two nondimensional factors due to the second mode conversion at point B (See Appendix B) with $\beta = 0.778$, and $\gamma = 2.3$.

Eqs. (5)–(7) indicate that point A is under tensile loading, point B is under mixed-mode loading. For the current sample dimensions, however, the interfacial shear stress is much higher than the normal stress ($\tau^S_{\text{int}}/\sigma^S_{\text{int}} = u_{\|}/u_{\perp} = \gamma = 2.30$). In order to obtain a pure shear-mode loading, the sample shown in Fig. 5 may be cut perpendicular to the propagation direction of shear wave S around point B. Alternatively, θ_1 could be chosen to be greater, i.e., $\theta_1 = 57.7°$. Details of the mixed-mode loading experimental design are reported in Wang (2002) and Wang et al. (2003a).

3.2. Mixed-mode interfacial strength of Al/fused silica interface

Interferometric measurements were carried out on samples with aluminum test film thicknesses between 0.5 and 1.0 μm. To accurately quantify the interfacial stress at film failure, the Argon detection beam was focused at point B (Fig. 5), the center of shear wave arrival, where the film failure was initiated. Typical interferometric data obtained on a 1.0 μm thick Al film at point B at 60% of full YAG power (0.140 J/mm^2) are shown in Fig. 6. Based on the geometry of the sample and the wave speeds in fused silica, the shear wave arrival at point B is expected at 754 ns after firing the Q switch of the YAG laser ($t = 0$). The interferometric signal in Fig. 6 shows the expected shear arrival at $t_3 = 754$ ns. The data also show the arrivals of some low-amplitude stresses at about $t_1 = 384$ ns and $t_2 = 604$ ns. Previous investigations (Wang et al., 2003a) showed that these waves are diagonally propagating longitudinal and shear waves travelling directly from the YAG deposition position (point C) to point B on the film surface (Fig. 5). The diagonal waves are significantly weaker than the expected shear wave S and do not influence film failure. Unfortunately, the diagonal shear wave arrival at t_2 overlaps with the expected longitudinal wave L_2, prohibiting the direct measurement of L_2. The shear wave S is not compromised by the diagonal waves and is measured.

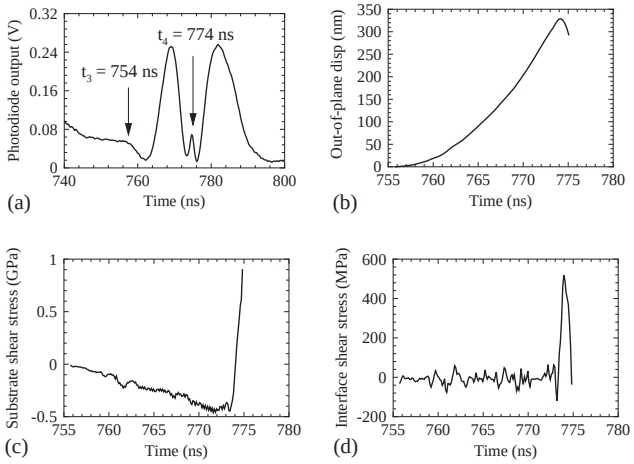

Fig. 7. Interferometric measurements obtained on a 1.0 μm thick Al film at point B: (a) fringe data (expanded view of the shear wave signal in Fig. 6); (b) out-of-plane displacement, $u_{\perp}$; (c) substrate shear stress, τ^{S}_{sub} and (d) interface shear stress, τ^{S}_{int}.

An expanded view of the shear wave signal in Fig. 6 is shown in Fig. 7a. The signal clearly shows tightening of fringe spacing (indicating acceleration in wave velocity) and a sudden turning at $t_4 = 774$ ns. The out-of-plane displacement is obtained from the voltage by fringe counting (as before, one fringe corresponds to half wavelength out-of-plane motion) (Wang et al., 2002), and is shown in Fig. 7b. These displacements are identified as associated with shear wave S by their time of arrival. The data processing associated with the shear wave arrival is taken from the fringe data near t_4. The substrate and interface shear stress are calculated from the displacement using Eqs. (3) and (4) and shown in Figs. 7c and d, respectively. Due to the acceleration and the sudden turning in the fringe signal, a linear ramp is present in the substrate stress profile with a peak stress of 0.47 GPa and followed by a sharp shock right at the turning. The stress profile is similar to that shown in Fig. 2b. After mode converting at the oblique surface, the stress wave has retained the characteristics of the shock developed in the initial longitudinal propagation L_1. The maximum interface shear stress resulting from the shock is 537 MPa as shown in Fig. 2d. The noise in Figs. 7c and d is due to the numerical differentiation of the displacement profile. The associated tensile stress (not shown in Fig. 7) at point B is 233 MPa as calculated from Eq. (7).

At the stress level reported in Fig. 7, a small amount of film failure was initiated (indicated by slight wrinkling at the edge of the loading spot). Significant damage, however, is observed when the films are tested under higher YAG laser power. Similar to the tensile case, the amount of the damage depends on the applied laser power, the test film thickness, and the waterglass confining layer thicknesses. More damage occurred at higher laser power in thicker films with thicker waterglass layers. Fig. 8 contains two optical microphotographs of a 1.2 μm thick damaged film near

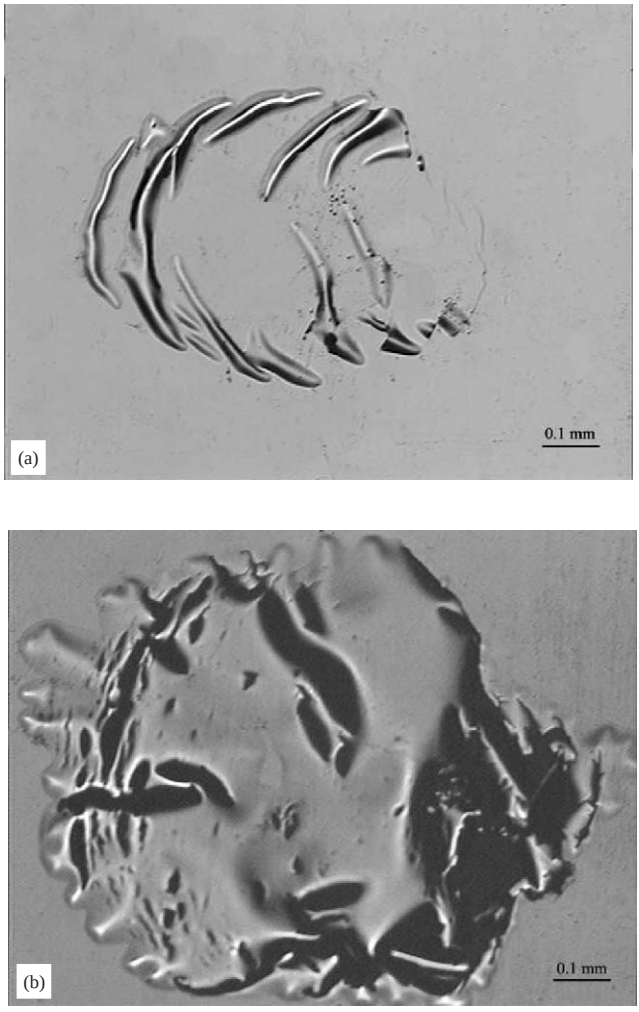

Fig. 8. Typical failure patterns observed on a 1.2 μm aluminum film in the mixed-mode loading experiment at 80% of full laser power; (a) waterglass confining layer thickness is 4 μm and (b) waterglass confining layer thickness is 6 μm. The horizontal direction in the microphotograph here corresponds to the direction A → B of Fig. 2. B is at the center of the damage and A is to the left.

point B at 80% of the full YAG power, but with two different waterglass confining layer thicknesses, 4 and 6 μm, respectively. It is clear that the film has failed in shear. The film damage and failure mode are significantly different from that observed for the tensile film spallation as shown in Fig. 4. In the shear case, the failed film is wrinkled and torn in sections. While under tensile loading the film lifted off the surface in a blister-like fashion. The direction of the wrinkling in Fig. 8 provides additional evidence that the failure is caused by a shear wave.

Table 4
Mixed-mode interfacial strength of aluminum film deposited on fused-silica substrates

Film thickness (μm)	Laser fluence (J/mm^2)	Sub_shear stress τ^S_{sub} (GPa)	Inter_shear stress τ^S_{int} (MPa)	Inter_normal stress σ^S_{sub} (MPa)
1.0	0.084	−0.42	537	233
	0.084	−0.39	562	244
	0.084	−0.39	562	244
0.8	0.112	−0.43	576	250
	0.084	−0.39	450	196
	0.084	−0.39	450	196
0.68	0.112	−0.43	490	213
	0.112	−0.43	490	213
Range			450–576	196–250
Average			523 ± 52	227 ± 23

After optimizing the confining layer thickness, which was found to be around 4 μm, measurements of the mixed-mode interfacial strength of Al/fused silica interface were performed for three film thicknesses, 0.68, 0.8 and 1.0 μm. The interfacial shear stress obtained from eight measurements (two on 0.68 μm, two on 0.8 μm and three on 1.0 μm) at film failure initiation are summarized in Table 4.[1] The average interfacial shear stress at failure is 523 ± 52 MPa associated with a simultaneous normal stress of 227 ± 23 MPa. These error bars are standard deviation of the measured values. Interfacial strength was obtained by gradually tuning up the YAG laser power until a small amount of film wrinkling was observed. The mixed-mode interfacial strength is higher than the tensile strength of the same interface reported in Section 2.2.

4. Discussion

The strength of an ideal thin film interface, Al film/fused silica substrate, was investigated under both tensile and mixed-mode loading conditions. Tensile parametric studies revealed important design parameters for improving the existing tensile spallation setup as well as developing the mixed-mode loading technique. Tensile interfacial strength was measured for a range of film and substrate thicknesses. Strength values were consistent, indicating that the measurement was independent of experimental parameters. Moreover, interfacial failure correlated with interface stress only. After optimizing the

[1] Failure in mixed mode was usually associated with a significant film displacement at or immediately after failure. As the interferometer measures film motion, not substrate motion, failure can mask the substrate velocity turn-around whose identification is critical for assessing interface stress. In order to more accurately assess interface stress at failure, interface stress on a nonfailing 0.2 μm test film was measured as a function of laser fluence. Then interface stress at failure of thicker films was inferred by referring to the calibration and correcting for the different test film thickness.

parameters governing the wave generation, propagation and detection mechanism, a shear wave with large enough stress to fail an aluminum film/fused silica interface was obtained. Quantitative data revealed that the mixed-mode interfacial strength was larger than tensile values for the same interface. This observation is consistent with the quasi-static mixed-mode experiments on bi-layer samples (Hutchinson and Suo, 1992; Liechti and Chai, 1991), in which interfacial fracture energy was found to increase with increasing mode II component.

The failure patterns observed under mixed-mode loading (mostly shear mode) were different from those observed in the tensile spallation experiment. Significant wrinkling and tearing occurred in the films due to the shear loading. These wrinkled patterns indicated that the failure mechanism of the film interface was mixed-mode decohesion.

The mixed-mode loading technique developed in this research can be used to investigate the interfacial strength for a range of mode-mixities. By a systematical changing of the incident angle θ_1 in Fig. 5, which will also subsequently change the mode conversion of the incident longitudinal wave to a shear wave, the interfacial strength could be measured for a full range of mixed-mode loading conditions from purely tensile to purely shear. The results may provide significant insights into thin-film failure mechanisms.

In this research, the interfacial adhesion strength is characterized in terms of stress. In many other adhesion measurement techniques, such as the scratch (Laugier, 1981), blister (Gent and Lewandowski, 1987) and indentation tests (Kriese et al., 1999a,b), the adhesion is measured in terms of energy. In order to relate measurements from the laser-spallation technique to that obtained from other techniques, future work can be carried out to calculate the energy associated with laser spallation. One such parameter that readily obtainable is the kinetic energy stored in the thin film, which is directly calculated from the measured surface velocity of the film, the film density, and thickness. Since this energy contains all the energy available in the film, it can serve as an upper bound for the fracture energy in the laser-spallation experiment.

The aluminum/fused-silica substrate was studied as a model system. Previous experimental investigations revealed that fused-silica substrates, with their negative nonlinear elasticity, caused the compressive stress wave generated by the pulsing laser to evolve a decompression shock, which was critical for generation of the fast fall times needed for significant loading of thin-film interfaces. By inserting an extra layer of the desired substrate material between the fused silica and the thin film, the current technique can be used to test a variety of substrates and films, especially those of interest to the microelectronics industry, such as polyimide, copper, aluminum and polysilicon on single-crystal silicon substrates. Overall, the use of laser-generated shear waves provides a new tool to explore a range of thin-film interfacial failure modes as well as the role of such extrinsic effects as residual stress, surface roughness, and imperfections.

5. Conclusions

Laser induced stress waves were used to characterize intrinsic interfacial strength of thin films under both tensile and mixed-mode conditions. A careful series of

experiments and analysis was carried out to optimize both the tensile and mixed-mode loading techniques. The interfacial tensile strength of an aluminum thin film on a fused silica substrate was measured for a range of different film and substrate thicknesses. A consistent tensile strength value of 490 ± 70 MPa was obtained, and the film failure correlated with interface stress only. Mixed-mode loading was achieved by allowing the laser-induced compression pulse to mode convert at an oblique surface, and the resulting shear wave to impinge upon the test film interface. Interfacial strengths obtained for Al film/fused silica substrate interfaces loaded in mixed-mode, a shear stress of 523 ± 52 MPa associated with a simultaneous normal stress of 227 ± 23 MPa, were higher than those obtained for the same films loaded by a tensile wave. The failure modes under mixed-mode loading were also quite different from that observed under pure tensile loading. Significant wrinkling and tearing occurred due to the in-plane shear wave loading. Hence, the loading mode played a critical role in determining the sequence of events leading to film failure.

Acknowledgements

The support of the University of Illinois Research Board and the National Science Foundation through grant CMS-99-88127 is gratefully acknowledged. The authors acknowledge the use of the Frederick Seitz Materials Research Lab and the Beckman Institute facilities at the University of Illinois.

Appendix A. Stress calculation using wave transmission and reflection coefficients

While the simplified stress calculation Eqs. (1) and (2) works well for small film thickness h (smaller than the wave speed times the rise time of the stress pulse), it may break down at certain large thicknesses. Here, standard wave transmission and reflection theory is adopted (Graff, 1991) to obtain an exact expression of the stress in the substrate and at the interface in terms of the measured surface displacement u_0. The substrate is considered as a homogeneous, isotropic semi-infinite media and the film of thickness h and different material properties is to be attached to the surface of the semi-infinite media as show in Fig. 9. In the analysis, $\lambda_1, \mu_1, \rho_1, c_1$ and $\lambda_2, \mu_2, \rho_2, c_2$ are the *Lamé* moduli, density and dilatational wave speed of the substrate and film, respectively.

Assuming a plane harmonic wave strikes the interface from the negative infinity, the one-dimensional elastic wave equation in both media is

$$(\lambda + 2\mu)_i \frac{\partial^2 u_i}{\partial x^2} = \rho_i \frac{\partial^2 u_i}{\partial t^2}. \tag{A.1}$$

The stress–displacement relation is given by

$$\sigma_i = (\lambda + 2\mu)_i \frac{\partial u_i}{\partial x}. \tag{A.2}$$

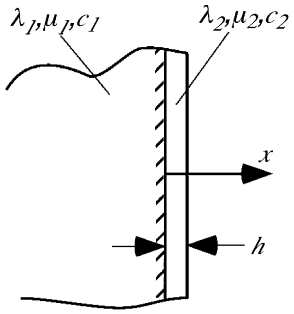

Fig. 9. A film of thickness h on a semi-infinite substrate.

The nontrivial boundary conditions for the problem are

$$u_1 = u_2, \quad \sigma_1 = \sigma_2 \quad \text{at} \quad x = 0, \tag{A.3}$$

$$u_2 = u_{\text{surface}} = u_0, \quad \sigma_2 = 0 \quad \text{at} \quad x = h. \tag{A.4}$$

Solutions to Eq. (A.1) can be obtained in the form of

$$\begin{aligned} u_1 &= A_1 e^{-i\omega(t+x/c_1)} + A_2 e^{-i\omega(t-x/c_1)}, \\ u_2 &= A_3 e^{-i\omega(t+x/c_2)} + A_4 e^{-i\omega(t-x/c_2)}. \end{aligned} \tag{A.5}$$

The corresponding stress can be written in the form

$$\begin{aligned} \sigma_1 &= -i\omega\rho_1 c_1 \left[A_1 e^{-i\omega(t+x/c_1)} - A_2 e^{-i\omega(t-x/c_1)}\right], \quad x \leqslant 0, \\ \sigma_2 &= -i\omega\rho_2 c_2 \left[A_3 e^{-i\omega(t+x/c_2)} - A_4 e^{-i\omega(t-x/c_2)}\right], \quad x > 0. \end{aligned} \tag{A.6}$$

By applying the boundary conditions Eq. (A.3) at the interface and Eq. (A.4) at the free film surface, one obtains

$$\begin{Bmatrix} A_1 \\ A_2 \\ A_3 \\ A_4 \end{Bmatrix} = \frac{\tilde{u}_0}{2} \begin{Bmatrix} \cos\dfrac{\omega h}{c_2} + i\dfrac{\rho_2 c_2}{\rho_1 c_1}\sin\dfrac{\omega h}{c_2} \\ \cos\dfrac{\omega h}{c_2} - i\dfrac{\rho_2 c_2}{\rho_1 c_1}\sin\dfrac{\omega h}{c_2} \\ \cos\dfrac{\omega h}{c_2} + i\sin\dfrac{\omega h}{c_2} \\ \cos\dfrac{\omega h}{c_2} - i\sin\dfrac{\omega h}{c_2} \end{Bmatrix}. \tag{A.7}$$

The amplitude of the incident stress in the substrate is therefore given by

$$\begin{aligned} \tilde{\sigma}_{\text{sub}} &= i\omega\rho_1 c_1 A_2 \\ &= \frac{\tilde{u}_0}{2}(i\omega)\rho_1 c_1 \left[\cos\frac{\omega h}{c_2} - i\frac{\rho_2 c_2}{\rho_1 c_1}\sin\frac{wh}{c_2}\right] \end{aligned} \tag{A.8}$$

and the amplitude of the stress acting on the interface is given by

$$\begin{aligned}\tilde{\sigma}_{\text{int}} &= -\mathrm{i}\omega\rho_2 c_2(A_3 - A_4)\\ &= \omega\rho_2 c_2\tilde{u}_0 \sin\frac{\omega h}{c_2}\\ &= -(\mathrm{i}\omega)^2\rho_2 c_2\tilde{u}_0\frac{\sin\omega h/c_2}{\omega}.\end{aligned} \tag{A.9}$$

For small film thickness h, $\cos wh/c_2 \approx 1$, $\sin wh/c_2 \approx 0$, then

$$\tilde{\sigma}_{\text{sub}} \approx (\mathrm{i}\omega)\rho_1 c_1\frac{\tilde{u}_0}{2}, \tag{A.10}$$

$$\tilde{\sigma}_{\text{int}} \approx \omega^2\rho_2 h\tilde{u}_0 = -(\mathrm{i}\omega)^2\rho_2 h\tilde{u}_0. \tag{A.11}$$

By inverse Fourier transformation, one obtains

$$\sigma_{\text{sub}} = -\frac{1}{2}(\rho_1 c_1)\frac{\partial u_0}{\partial t}, \tag{A.12}$$

$$\sigma_{\text{int}} = -\rho_2 h\frac{\partial^2 u_0}{\partial t^2}. \tag{A.13}$$

which are the same as Eqs. (1) and (2).

Without the assumption of small film thickness h, Eq. (A.8) leads to the following expressions

$$\sigma_{\text{sub}} = -\frac{1}{2}\frac{\partial}{\partial t}\left\{u_0 * \left[\rho_1 c_1\mathrm{IFT}\left(\cos\frac{wh}{c_2}\right) - \mathrm{i}\rho_2 c_2\mathrm{IFT}\left(\sin\frac{\omega h}{c_2}\right)\right]\right\}, \tag{A.14}$$

$$\sigma_{\text{int}} = -\rho_2 c_2\frac{\partial^2}{\partial t^2}\left[u_0 * \mathrm{IFT}\left(\frac{\sin\frac{\omega h}{c_2}}{\omega}\right)\right], \tag{A.15}$$

where IFT denotes the inverse Fourier transformation, and

$$\mathrm{IFT}\left(\cos\frac{\omega h}{c_2}\right) = \frac{1}{2}\left[\delta\left(t - \frac{h}{c_2}\right) + \delta\left(t + \frac{h}{c_2}\right)\right],$$

$$\mathrm{IFT}\left(\sin\frac{\omega h}{c_2}\right) = \frac{\mathrm{i}}{2}\left[\delta\left(t - \frac{h}{c_2}\right) - \delta\left(t + \frac{h}{c_2}\right)\right],$$

$$\mathrm{IFT}\left(\frac{\sin\omega h/c_2}{w}\right) = \begin{cases}\sqrt{\dfrac{\pi}{2}} & |t| \leqslant \dfrac{h}{c_2},\\ 0 & \text{otherwise.}\end{cases}$$

Eqs. (A.14) and (A.15) yield the final expression for substrate and interface stress

$$\sigma_{\text{sub}} = -\frac{\rho_1 c_1}{4}\frac{\partial}{\partial t}\left\{u_0 * \left[\delta\left(t - \frac{h}{c_2}\right) + \delta\left(t + \frac{h}{c_2}\right)\right]\right\}$$

$$
\begin{aligned}
&- \frac{\rho_2 c_2}{4} \frac{\partial}{\partial t} \left\{ u_0 * \left[\delta\left(t - \frac{h}{c_2}\right) - \delta\left(t + \frac{h}{c_2}\right) \right] \right\} \\
&= - \frac{\rho_1 c_1}{4} \frac{\partial}{\partial t} \left\{ \left[u_0\left(t - \frac{h}{c_2}\right) + u_0\left(t + \frac{h}{c_2}\right) \right] \right\} \\
&\quad - \frac{\rho_2 c_2}{4} \frac{\partial}{\partial t} \left\{ \left[u_0\left(t - \frac{h}{c_2}\right) - u_0\left(t + \frac{h}{c_2}\right) \right] \right\}, \qquad \text{(A.16)}
\end{aligned}
$$

$$
\begin{aligned}
\sigma_{\text{int}} &= -\rho_2 c_2 \frac{\partial^2}{\partial t^2} \left\{ u_0 * \sqrt{\frac{\pi}{2}} \left[H\left(t - \frac{h}{c_2}\right) - H\left(t + \frac{h}{c_2}\right) \right] \right\} \\
&= -\rho_2 c_2 \sqrt{\frac{\pi}{2}} \frac{\partial^2}{\partial t^2} \int_{-h/c_2}^{h/c_2} u_0(t + \xi)\, \mathrm{d}\xi, \qquad \text{(A.17)}
\end{aligned}
$$

which are valid for large film thickness.

Appendix B. Mode-conversion in mixed-mode loading experiment

Refer to Fig. 5, the displacement amplitudes of the incident longitudinal, reflected longitudinal and shear waves in the substrate are denoted with u_{L_1}, u_{L_2} and u_S. According to standard wave propagation theory (Graff, 1991), the mode-conversion coefficients are expressed as

$$
\frac{u_{L_2}}{u_{L_1}} = \frac{\sin 2\theta_1 \sin 2\theta_2 - k^2 \cos^2 2\theta_2}{\sin 2\theta_1 \sin 2\theta_2 + k^2 \cos^2 2\theta_2}, \qquad \text{(B.1)}
$$

$$
\frac{u_S}{u_{L_1}} = \frac{2k \sin 2\theta_1 \cos 2\theta_2}{\sin 2\theta_1 \sin 2\theta_2 + k^2 \cos^2 2\theta_2}, \qquad \text{(B.2)}
$$

where $k = c_L/c_S$ is the ratio of longitudinal and shear wave speeds, and θ_2 is given by Snell's law

$$
\frac{\sin\theta_1}{\sin\theta_2} = k. \qquad \text{(B.3)}
$$

For fused silica, $k \approx 1.584$. At an angle of $\theta_1 = 45°$, the mode-conversion coefficient u_S/u_{L_1} reaches its maximum.

When shear wave S reaches the test film surface at point B, it will be mode-converted again into a shear wave S' and a longitudinal wave L_3 as shown in Fig. 10. The incident angles of waves S' and L_3 are θ_3 and θ_4, respectively. From Snell's law,

$$
\frac{\sin\theta_4}{\sin\theta_3} = k, \qquad \text{(B.4)}
$$

$\theta_4 \approx 30.17°$. The out-of-plane and in-plane displacements at point B are denoted $u_\perp$ and $u_\parallel$, respectively. For an incident shear wave S with displacement amplitude u_S, the out-of-plane displacement at point B is obtained from basic wave-propagation theory

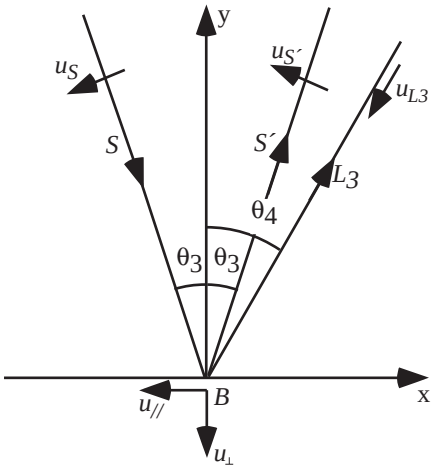

Fig. 10. Mode conversion at point B.

(Graff, 1991),

$$u_\perp = u_s\beta, \tag{B.5}$$

where

$$\beta = \frac{k\sin 4\theta_3\cos\theta_4 + 2\sin 2\theta_3\sin 2\theta_4\sin\theta_3}{\sin 2\theta_3\sin 2\theta_4 + k^2\cos^2 2\theta_2}. \tag{B.6}$$

The ratio between the in-plane and out-of-plane displacement components at point B is

$$\frac{u_\parallel}{u_\perp} = \frac{k\sin 4\theta_3\sin\theta_1 + 2k^2\cos^2 2\theta_3\cos\theta_3}{k\sin 4\theta_3\cos\theta_4 + 2\sin 2\theta_4\sin 2\theta_3\sin\theta_3} := \gamma. \tag{B.7}$$

For the current geometry, $\beta \approx 0.778$ and $\gamma \approx 2.30$.

References

Alexopoulos, P.S., O'Sullivan, T.C., 1990. Mechanical properties of thin films. Annu. Rev. Mater. Sci. 20, 391–420.

Archer, P., Gupta, V., 1998. Measurement and control of ice adhesion to aluminum 6061 alloy. J. Mech. Phys. Solids 46 (10), 1827–1837.

Baglin, J.E.E., Clark, G.J., 1985. Ion beam bonding of thin films. Nucl. Instrum. Methods in Phys. Res. B7/8, 881–885.

Barker, L.M., Hollenbach, R.E., 1970. Shock wave studies of PMMA, fused silica and sappire. J. Appl. Phys. 41, 4208–4226.

Boustie, M., Auronz, E., Romain, J.P., Bertoli, A., Manesse, D., 1999. Determination of the bond strength of some micron coatings using the laser shock technique. Epj Appl. Phys. AP5, 149–153.

Cao, H.C., Evans, A.G., 1989. An experimental study of the fracture resistance of bimaterial interfaces. Mech. Mater. 7, 295–305.

Charalambides, P.G., Lund, J., Evans, A.G., McMeeking, R.M., 1989. A test specimen for determining the fracture resistance of bimaterial interfaces. J. Appl. Mech. 56, 77–82.

Chu, Y.Z., Jeong, H.S., White, R.C., Durning, C.J., 1992. Characterization of adhesion in thin-film materials by the blister test. MRS Symposium Proceedings, Vol. 276, pp. 209–220.

Evans, A.G., Bartlett, A., Davis, B., Flinn, B.D., Turner, M., Reimanis, I.E., 1991. Fracture resistance of metal/ceramic/intermetallic interfaces. Scr. Metal. Mater. 25 (5), 1003–1010.

Evans, A.G., Hutchinson, J., 1995. The thermomechanical integrity of thin films and multilayers. Acta Metall. Mater. 43, 2507–2530.

Gent, A.N., Lewandowski, L.H., 1987. Blow-off pressures for adhering layers. J. Appl. Polymer Sci. 33, 1567–1577.

Graff, K., 1991. Wave Motion in Elastic Solids. Dover, New York.

Gupta, V., Yu, A., 1997. Characterizing adhesion of thermal barrier coatings. Compos. Functionally Graded Mater. 80, 399–400.

Gupta, V., Yuan, J., 1993. Measurement of interface strength by the modified laser-spallation technique: II. Applications to metal/ceramic interfaces. J. Appl. Phys. 74, 2397–2404.

Gupta, V., Argon, A.S., Cornie, J.A., Parks, D.M., 1990. Measurement of interface strength by laser pulse-induced spallation. Mater. Sci. Eng. A 125, 105–117.

Gupta, V., Argon, A.S., Parks, D.M., Cornie, J.A., 1992. Measurement of interface strength by a laser spallation technique. J. Mech. Phys. Solids 40, 141–180.

Gupta, V., Yuan, J., Pronin, A., 1994. Recent developments in the laser spallation technique to measure the interface strength and its relationship to interface toughness with applications to metal/ceramic, ceramic/ceramic and ceramic/polymer interfaces. J. Adhes Sci. Technol. 8, 713–747.

Gupta, V., Hernandez, R., Wu, J., Charconnet, P., 2000. Interfacial adhesion and its degradation in selected metal/oxide and dielectric/oxide in multi-layer devices. Vacuum 59 (1), 292–300.

Heavens, O.S., 1950. Some factors influencing the adhesion of films produced by vacuum evaporation. J. Phys. Radium 11, 355–360.

Hull, T.R., Colligon, J.S., Hill, A.E., 1987. Measurement of thin film adhesion. Vacuum 37, 327–330.

Hutchinson, J.W., Suo, Z., 1992. Mixed-mode cracking in layered materials. Adv. Appl. Mech. 29, 63–191.

Jacobsson, R., Kruse, B., 1973. Measurement of adhesion of thin evaporated films glass substrates by means of the direct pull method. Thin Solid Films 15 (1), 71–77.

Kim, K.S., Kim, J., 1988. Elasto-plastic analysis of the peel test for thin film adhesion. J. Eng. Mater. Technol.-Trans. ASME 110 (3), 266–273.

Kriese, M.D., Gerberich, W.W., Moody, N.R., 1999a. Quantitative adhesion measures of multilayer films: Part I. Indentation mechanics. J. Mater. Res. 14 (7), 3007–3018.

Kriese, M.D., Gerberich, W.W., Moody, N.R., 1999b. Quantitative adhesion measures of multilayer films: Part II. Indentation of W/Cu, W/W, Cr/W. J. Mater. Res. 14 (7), 3019–3026.

Laugier, M., 1981. The development of the scratch technique for the determination of the adhesion of coatings. Thin Solid Films 76 (3), 289–294.

Liechti, K.M., Chai, Y.S., 1991. Biaxial loading experiments for determining interfacial fracture toughness. J. Appl. Mech. 58 (3), 680–687.

Mattox, D.M., 1978. Adhesion measurement of thin films, thick films and bulk coatings, Am. Soc. Test. Mater. Spec. Tech. ASTM, Philadelphia.

Miklowitz, J., 1978. Elastic Waves and Waveguides. North-Holland, Amsterdam.

Mittal, K.L., 1978. Adhesion measurement: recent progress, unsolved problems, and prospects. Adhesion Measurement of Thin Films, Thick Films, and Bulk Coatings, ASTM STP 640, American Society for Testing and Materials, Philadelphia, pp. 5–17.

Mittal, K.L., 1987. Selected bibliography on adhesion measurement of films and coatings. J. Adhes. Sci. Technol. 1 (3), 247–259.

Sbaizero, O., Charalambides, P.G., Evans, A.G., 1990. Delamination cracking in a laminated ceramic matrix composite. Appl. Mech. Rev. 43, 1936–1940.

Strong, J., 1935. On the cleaning of surfaces. Rev. Sci. Instrum. 6, 97–98.

Thouless, M.D., 1990. Fracture mechanics of a model interface under mixed-mode loading. Acta Metall. 38, 1135–1140.

Thouless, M.D., 1994. Fracture mechanics for thin film adhesion. IBM J. Res. Dev. 38, 367–377.

Turner, M.R., Evans, A.G., 1996. Experimental study of the mechanisms of crack extension along an oxide/metal interface acta materialia. Appl. Mater. Res. 44 (3), 863–871.

Vossen, J.L., 1978. Measurements of film–substrate bond strength by laser spallation. Adhesion Measurement of Thin Films, Thick Films and Bulk Coatings ASTM STP 640, American Society for Testing and Materials, Philadelphia, pp. 122–123.

Wang, J., 2002. Thin film adhesion measurement by laser induced stress waves. Ph.D. Thesis, University of Illinois.

Wang, J.S., Suo, Z., 1990. Experimental determination of interfacial toughness using brazil-nut-sandwich. Acta Metall. 38, 1279–1290.

Wang, J., Weaver, R.L., Sottos, N.R., 2002. A parametric study of laser induced thin film spallation. Exp. Mech. 42 (1), 74–83.

Wang, J., Sottos, N.R., Weaver, R.L., 2003a. Mixed-mode failure of thin films using laser generated shear waves. Exp. Mech. 43 (3), 323–330.

Wang, J., Weaver, R.L., Sottos, N.R., 2003b. Laser induced decompression shock development in fused silica. J. Appl. Phys. 93 (12), 9529–9536.

Weaver, C., 1975. Adhesion of thin films. J. Vac. Sci. Technol. 12, 18–25.

Yang, L.C., 1974. Stress waves generated in thin metallic films by a Q-switched ruby laser. J. Appl. Phys. 45 (6), 2602–2608.

Yu, A., Gupta, V., 1998. Measurement of in situ fiber/matrix interfacial strength in graphite/epoxy composites. Compos. Sci. Technol. 58 (11), 1827–1837.

Yuan, J., Gupta, V., 1993. Measurement of interface strength by the modified laser-spallation technique: I. Experiment and simulation of the spallation process. J. Appl. Phys. 74, 2388–2396.

Yuan, J., Gupta, V., Pronin, A., 1993. Measurement of interface strength by the modified laser-spallation technique: III. Experimental optimization of the stress pulse. J. Appl. Phys. 74, 2405–2410.